

Multi-Parameter Geophysical Observatory: gateway to integrated earthquake precursory research

B. R. Arora*, Gautam Rawat, Naresh Kumar and V. M. Choubey

To study earthquake precursors in an integrated manner, India's first Multi-Parameter Geophysical Observatory (MPGO) has been established at Ghuttu, Central Himalaya. The MPGO is located in a narrow belt of high seismicity where the colliding Indian–Asian plates are locked and are accumulating strains for future great earthquakes. The observatory is equipped with a superconducting gravimeter, overhauser and fluxgate magnetometers, ULF band search coil magnetometer, GPS, radon and water-level recorders. Supplemented by the dense network of broadband seismometers, the MPGO is designed to record precursory signals resulting from stress-induced changes in density, magnetization, resistivity, seismic wave velocity, fracture propagation, crustal deformation, electromagnetic and radon gas emission as well as fluctuations in hydrological parameters. The immediate priority for the characterization of precursory signals is to develop techniques to estimate and eliminate the background variation caused by the hydrological, environmental and solar terrestrial dynamics related changes. A careful scrutiny of the data associated with the Kharsali earthquake ($M_L = 4.9$) of 22 July 2007, revealed unambiguous co-seismic gravity jump perhaps related to the change in volumetric strain. Similarly, radon fluxes show some definite trend that can be viewed as pre- and co-seismic changes related with the Kharsali earthquake. Sudden drop of geomagnetic field intensity and dynamic waveform, lasting from several days before to a week after the earthquake, appears to be a manifestation of the thermal agitation on the magnetization of rocks around the source region of the earthquake. A new method of location of seismo-EM source has been developed and its efficacy demonstrated in the seismically active Koyna region. The results obtained so far show that the multi-parameter approach crafted by the Ministry of Earth Sciences under the National Program on Earthquake Precursors holds promise and long-term monitoring needs to be continued for statistical validation.

Keywords: Dilatancy–diffusion, earthquake precursors, radon changes, seismomagnetism, short-term prediction.

HYPOTHESIS of seismic gap, earthquake recurrence and progressive failure coupled with improved understanding of the tectonics and dynamics of the plate boundaries allows demarcation of segments of seismic belts preparing for future large/great earthquakes^{1–3}. This is a significant step towards long-term earthquake prediction on the timescale of 10–100 years. Applications of the principle of chaotic theory to the instrumentally recorded earthquake data have also come to a stage where intermediate-term (1–10 years) prediction of earthquakes is claimed to

be at an advanced stage^{4–6}. Introduction of GPS measurements permitting reliable estimates on plate motion and accumulating strains has also begun to complement the prediction on long and intermediate term timescale^{7,8}. However, the status of short-term (days to hours) predictions that can lead to practical actions to save human life remains obscure. An overview of some successes and failed events⁹ indicates that the probability that an earthquake can be predicted successfully on short-term basis has oscillated between optimism and skepticism. The knowledge gaps in our understanding of the predictive tools were evident when the forecast of earthquake with $M > 6$ on the San Andreas Fault in the United States did not come true within the specified time window¹⁰. This virtually ruined the Parkfield prediction experiment wherein a wide array of geophysical instru-

B. R. Arora is in the Uttarakhand Council for Science and Technology, 6, Vasant Vihar Phase I, Dehradun 248 006, India; Gautam Rawat, Naresh Kumar and V. M. Choubey are in the Wadia Institute of Himalayan Geology, 33 GMS Road, Dehradun 248 001, India.

*For correspondence. (e-mail: arorabr47@gmail.com)

mentation was deployed to record earthquake precursors¹¹. Even when the predicted earthquake did occur in 2004, no precursors of significance were observed¹². Despite these early impediments, the quest for precursors and their documentation has continued in many active seismic zones of the world. As a result of the increased monitoring, there has been increased reporting of the variety of precursory signals, notable among them are enhanced foreshocks, seismicity pattern, crustal deformation, changes in groundwater, thermal anomalies in surface temperature, variation in radon/helium gas as well as localized changes in gravity, magnetic, electrical resistivity and electromagnetic emission in ULF bands, etc. Each of these parameters has some success stories in the sense that on retrospection the parameters revealed certain characteristic changes which one way or the other appeared to be related to earthquake occurrence. The natural time analysis of seismic electrical signals (SES) was used with partial success in issuing forecast of an earthquake in a narrow time window of a few hours to a few days^{13,14}. Pessimism prevailed¹⁵, as it has been noted that one particular precursor may not be observed at all earthquake sites, or even for different earthquakes in the same region. Fresh optimism is evidenced as synthesis of some widely reported precursory signals, e.g. SES, EM emission in the ULF band, groundwater and radon has begun to give insight on the dependence of the amplitude and duration of the precursors on the magnitude and distance of the impending earthquake¹⁶. The absence of a sound physical mechanism that links the given precursor to the earthquake rupture process adds to the skepticism and is a major barrier in the practical prediction programmes. Although as yet no precursor or class of precursors can be deterministic for short-term prediction, it is felt that some of the skepticism is ill-founded as large-scale, nationally funded programmes on prediction have relied on the expansion of the seismological network, while operational tools developed to monitor non-seismological precursors are still lacking¹⁷.

The dilatancy–diffusion model, based on the behaviour of crustal rocks under near-critical stress levels, remains the best working model to explain the existence of the reported precursors¹⁸. The model hypothesis that generation of various precursors is a sequential effect of the opening of minor cracks, influx of fluids and material strengthening that rocks exhibit when subjected to accumulating stresses simulating different phases of the earthquake preparatory cycle. The multiple physical models invoke influence of changing material state on the physical properties of the rocks to explain the generation of the reported precursors. Albeit there is no agreement about how the specific mechanisms operate to account for the particular features of field observations. Given that the number of parameters is expected to show distinct temporal changes during the earthquake preparatory cycles, their isolation against the natural background

variation and characterization of space–time pattern could be critical to help establish the operating physical mechanism and their validation against each other could as well be used to test their collective value in real-time forecast of the earthquake. Recognizing these, the Indian National Programme on Earthquake Prediction, launched by the Ministry of Earth Sciences, Government of India, has approved the establishment of Multi-Parameter Geophysical Observatories (MPGOs) for simultaneous measurements of inter-disciplinary parameters. The Wadia Institute of Himalayan Geology, Dehradun was entrusted with the responsibility of establishing an MPGO in Uttarakhand Himalaya for generating high-resolution data for integrated precursory research. In this article, we trace the rationale for selecting the site, geophysical instrumentation and initial processing strategies required to quantify the background variability as a step to isolate precursors. The observatory became fully functional in April 2007; the collected datasets are discussed to highlight quality and influence of hydrological and environmental parameters controlling the background variability against which precursory signals are isolated. Data in association with the M_w 5.0 Kharsali earthquake, the largest recorded since the inception of the Observatory are presented to illustrate the nature of precursory and co-seismic signals.

Ghuttu MPGO: site-selection consideration and configuration

The Himalaya is one of the most active seismic inter-continental regions where devastating earthquakes result due to the continued continent–continent collision between India and Asia. Recognizing the large seismic hazard of the Himalaya, the first Indian MPGO was established at Ghuttu (30.53°N, 78.74°E), Garhwal Himalaya, Uttarakhand (Figure 1). Longitudinally, Ghuttu is located in the central Himalaya seismic gap¹, bounded by the 1905 Kangra ($M \sim 7.8$) earthquake on the west and the 1934 Bihar–Nepal ($M \sim 8.3$) earthquake on the east (Figure 1a), where accumulated strains are estimated to be large enough to produce great earthquakes⁷. Further in a section across the Himalaya, the MPGO is located in a narrow Himalayan Seismic Belt (HSB; Figures 1b and 2), which is best seen as the locked section of the down-dip edge of the seismically active detachment¹⁹ or more simply the ramp structure between the seismically active detachment to the south and the aseismically slipping detachment to the north²⁰. The region has also been the seat of the recent 1991 Uttarkashi and 1999 Chamoli earthquakes, both $M > 6$, which exhibited a well-developed pattern of quiescence/accelerated seismicity that invariably precedes the large earthquakes²¹. In addition, precursory change in the b value and RTL anomaly has been identified in association with the 1999 Chamoli earth-

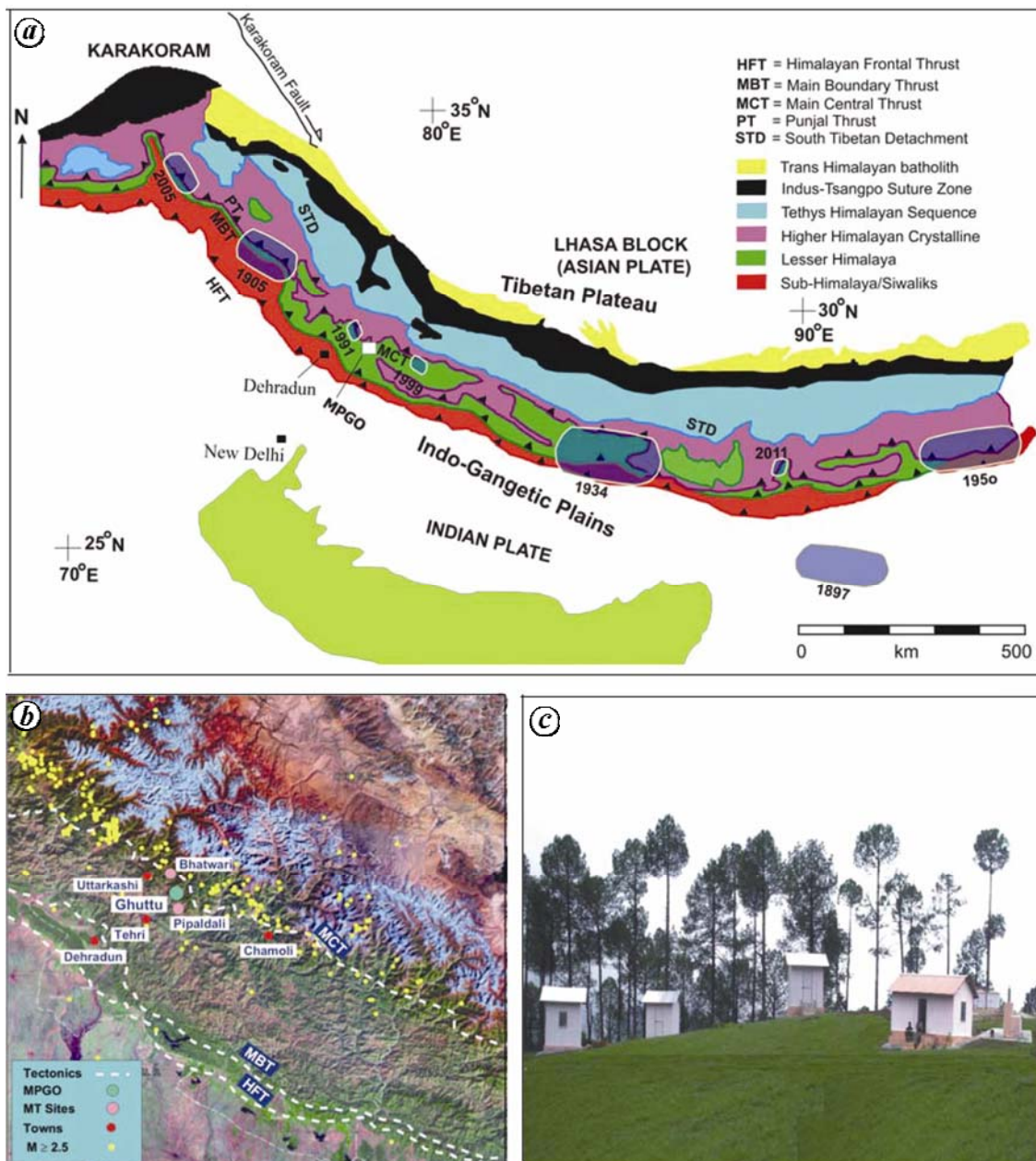


Figure 1. *a*, Location of the Multi-Parameter Geophysical Observatory (MPGO), Ghuttu in the backdrop of the tectonic framework and great and recent large earthquakes in the Himalaya. *b*, MPGO and the support magnetic stations at Bhatwari and Pipaldali in relation to narrow Himalayan seismicity belt of moderate earthquakes. *c*, Huts housing various equipment installed at MPGO.

quake²². In this seismotectonic perspective, the augon gneisses of the Higher Himalaya Complex exposed surrounding the Ghuttu window, provided the hard rock formation to house seismic, Global Position System (GPS) and gravity sensors to record data without much attenuation, thus ensuring high signal-to-noise ratio. The MPGO is equipped with a state-of-the-art superconducting gravimeter, overhauser magnetometer, ULF band search coil magnetometer, radon datalogger, water-level recorder and is backed by a dense network of GPS and broadband seismometers (BBS).

Seismicity

By design, the MPGO is located in the central part of the wide aperture BBS network in the Garhwal–Kumaon Himalaya that was developed in parallel to provide information on local seismicity in real mode. Inclusion of the data from this array has lowered the detection threshold of earthquakes in this section of the Himalaya from the cut-off value of $M = 4.3$ to 1.8. The distribution of earthquake epicentres from July 2007 to December 2010 helped define the HSB as a narrow belt straddling the sur-

face trace of the MCT (Figure 2). As noted earlier, the HSB is viewed as the locked portion of the down dip portion of the underthrusting Indian plate possibly marked by a ramp^{19,20}. Within this narrow belt, some anomalous clustering pattern is registered, the most prominent cluster is centred at Tapovan²³ (Figure 2). Within this cluster, separated by less than 50 km, two sequences of swarms were recorded, one near Tapovan during April 2009 and another near Gaurikund during May 2009. Both swarm sequences lasting for 7 days and only 9 h respectively, witnessed 46 and 15 events ranging between $1.8 \leq M \leq 2.8$. Studying space–depth–time distribution, both sequences have been shown to originate from the same source point and an area of 100×100 sq. km has been identified as the potential zone preparing for future earthquakes²³. The impact of such reinforcing of seismic networks in different parts of the globe has facilitated identification of anomalous seismicity pattern²⁴, nucleation²⁵ and zones of accelerating/decelerating rate²⁶, and their applications in practical short-term prediction of earthquakes have begun to appear on the scene^{6,27}.

Soon after the seismic network and the MPGO commenced operation, the Kharsali earthquake ($M_L = 4.9$ and $M_w = 5.0$) occurred on 22 July 2007 at 23:02:13.22 UTC. The earthquake with its epicentre at 30.91°N, 78.31°E was estimated to be located at the focal depth of 15 km. The fault plane solution favours the role of reverse fault movement with significant strike–slip component in the generation of the earthquake²⁸. The focal mechanism and depth support the hypothesis that the earthquake resulted due to thrust movement along the blind basement thrust marking transition between the

down-going Indian plate and the over-riding wedge of the Himalaya. The Kharsali earthquake being the largest earthquake since the recording of multi-disciplinary data commenced at MPGO, Ghuttu, the efficacy of different processing strategies being developed to isolate weak precursory is tested with respect to this earthquake.

Characterization of variability of geophysical time series

The high-precision equipments deployed have the requisite sensitivities to record characteristic stress-induced perturbations, but the isolation of weak precursory signals is still a challenge as each geophysical time series has characteristic time variability related to inter-planetary, terrestrial, hydrological, environmental and tectonic sources. The applications of data-adopted numerical techniques are critical to understand the sources and the nature of time variability of different geophysical time series. We illustrate this by discussing the complexities and gneisses of gravity and radon time series recorded at MPGO, Ghuttu.

Time-varying gravity field

The opening of cracks and influx of fluids in the dilatant zone of an impending earthquake are expected to perturb the mass distribution during the earthquake build-up cycle, which should be reflected in time-varying gravity field. With this rationale, the measurements of time-varying gravity field were recorded using a superconducting gravimeter (SG; supplied by M/s GWR, USA). This was India's first SG recording gravity field at sub- μGal level. Installation and operational details of SG at Ghuttu are given in Arora *et al.*²⁹. The SG recorded temporal variations in gravity in voltages, which were converted to nm/s^2 ($1 \text{ nm/s}^2 = 0.1 \mu\text{Gal}$) using the conversion factor obtained by parallel registration with an absolute gravimeter. This calibration became possible with support from the National Geophysical Research Institute, Hyderabad by facilitating parallel recordings with the absolute gravimeter SG-5 to an accuracy of $2 \mu\text{Gal}$. Such comparisons provided the best possible calibration as no other gravity-measuring instrument approaches the accuracy of SG. The performance and quality of the recorded data have been validated by comparing the amplitudes and phases of the spheroidal modes of the free oscillations of the earth with globally established values²⁹.

During the initial operational period, loss of temperature control on SG elements following prolonged power failure produced gaps and caused steps or shift in base level. Later, induction of more robust power back-up with regulated power greatly reduced the gaps and jumps in the data. The gravity recordings with 1 sample/sec were first repaired using 'tsoft' toolkit³⁰ to fill the gaps, adjust step jumps/shift and correct spurious spikes, etc. due to

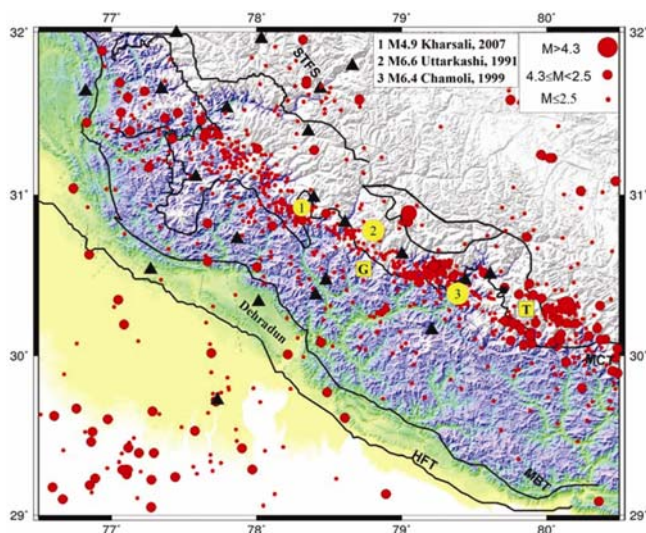


Figure 2. Distribution of earthquake epicentres recorded between July 2007 and December 2010 by a network of broadband seismometers around MPGO, Ghuttu (G). Epicentre of M_L 4.9 Kharsali earthquake (1) and centres of clustered seismicity around Tapovan (T) and Gaurikund (just west of epicenter zone (3) of the Chamoli earthquake) are also marked.

external mechanical noises. The data are then disseminated to produce 1-min values, wherein the high-frequency signals associated with the passage of seismic waves of local earthquakes are highly subdued. The long-period records of 1-min gravity observations are dominated by solid earth tides and contain the influence of atmospheric pressure, hydrological fluctuations, etc. (Figure 3, top). Using the global models of tidal attraction between the Earth–Moon–Sun systems, the observed variations are cleaned for tidal effects using the program ANALYSE from the ETERNA 3.3 package³¹. Following the globally accepted practice, pressure effects³² are eliminated using the admittance coefficient ($-0.32 \mu\text{Gal}/\text{hPa}$) established between earth tide-corrected gravity field and the concurrently recorded pressure variations (Figure 3, middle). The residual obtained after removing the tidal and pressure effects (Figure 3, bottom) shows variation of about $30\text{--}35 \mu\text{Gal}$. The residual gravity pattern with annual cycle was found to repeat during the observations of three consecutive years: 2007–2009 (Figure 4a). The correlation with recorded precipitation as well as groundwater level, measured in a 68 m deep borehole, shows strong influence of the hydrological cycle on the gravity field (Figure 4b and c). The gravity field begins to rise with the onset of rainfall and accompanying increase in the groundwater level. The amplitude of the gravity perturbation attains a peak value overlapping with intervals of continuous rainfall and when the groundwater level is shallowest in its periodic annual cycle (Figure 4). Precipitated water that reaches the ground surface is partially discharged as surface run-off, whereas a part infiltrates into the ground. The percolating water is stored in the top soil layer as soil moisture; bringing changes in the mass distribution and possibly affecting the gravity fields. Once the surface layer is saturated, the infiltrating water recharges the groundwater aquifer evidenced by rise in groundwater level. It can be hypothesized that slow seasonal gravity changes recorded

during the onset of the rainy season may be controlled by the combined effects of degree of soil saturation as well as the rate of recharge of aquifer. The decreasing gravity trend following the rainy season could be determined by the temperature controlled evaporation from moist soil as well as drop in water level due to discharge of the ground aquifer. That the two independent mechanisms are operative is evidenced by the transient steep changes in gravity in association with sporadic intense rainfall events during the dry period, which are not seen to affect the groundwater level. Given such a correspondence, a number of studies are devoted to detect and quantify the hydrological influence on high-precision gravity data^{33–36}.

In principle, the sensing device of the gravimeter being equivalent to a suspended pendulum, the signatures of the passing seismic waves on gravity records are marked as oscillatory signals whose amplitudes decay off with the passing away of the seismic waves. However, whether the entire spectrum of co-seismic oscillatory gravity variations is solely caused by the mechanical vibrations due to the passing seismic waves or drawing analogy with similar changes recorded in groundwater level of confined aquifer, it may contain manifestation of the pore-water pressure fluctuations in the aquifer to passing earthquake waves³⁷. This is an area of future studies. Nevertheless, a careful scrutiny of the residual gravity data sampled every second revealed unambiguous co-seismic jump of $5.2 \mu\text{Gal}$ in relation to the Kharsali earthquake ($M_L = 4.9$) of 22 July 2007 (Figure 5). Step gravity jumps are a persistent feature recorded by the network of SGs placed in different parts of the world^{38–40}. The spatial distribution of the magnitude of the static gravity jump recorded at three widely spaced SG stations in association with a large Tokachi-oki earthquake ($M_w = 8.0$) was found to be consistent with the estimates calculated based on simple dislocation on the fault³⁸. The proximity of the Ghuttu SG station to the epicentre of the Kharsali earthquake (only about 60 km), and their locations on either side of the causative fault, was conducive to produce large co-seismic gravity change by fault displacement, but the sign of the observed gravity jump is opposite to that expected by the up–dip displacement on a fault (V. M. Tewari, pers. commun.). The observed gravity jumps are co-seismic in the sense that they occur when earthquake waves arrive and pass beneath the SG station. It may be worthy to check whether the sense and magnitude of the gravity change is proportional to the volumetric strain released during earthquake⁴¹.

Radon and groundwater level variations

Since the 1966 Tashkent great earthquake⁴², anomalous changes in radon in association with earthquake occurrences are among the most widely researched parameters^{43–46}. Increased diffusion of radon from rocks in

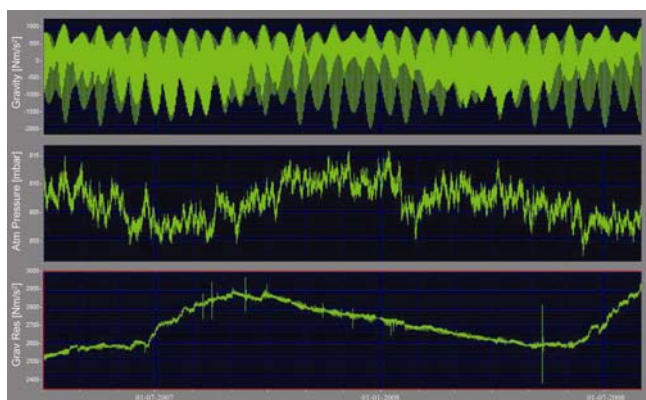


Figure 3. (Top) High-resolution time-varying gravity field recorded by the superconducting gravimeter at Ghuttu. (Middle) Atmospheric pressure and (bottom) residual gravity field obtained after removing the tidal and atmospheric pressure effects.

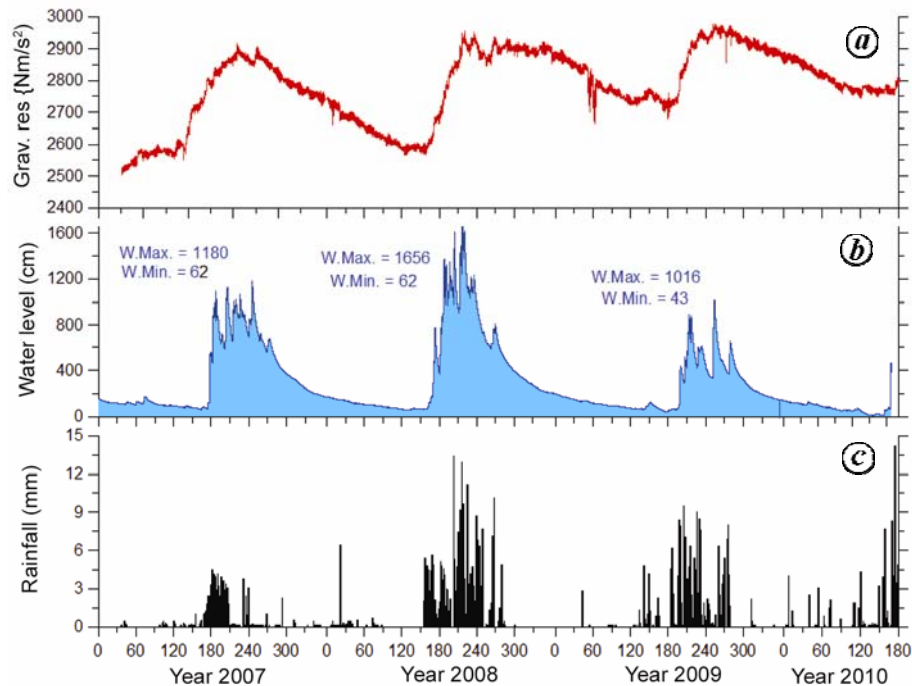


Figure 4. *a*, Residual gravity variations corrected for earth tide and atmospheric pressure variation together with the corresponding water-level fluctuations (*b*) and rainfall (*c*) during the period July 2007–2010.

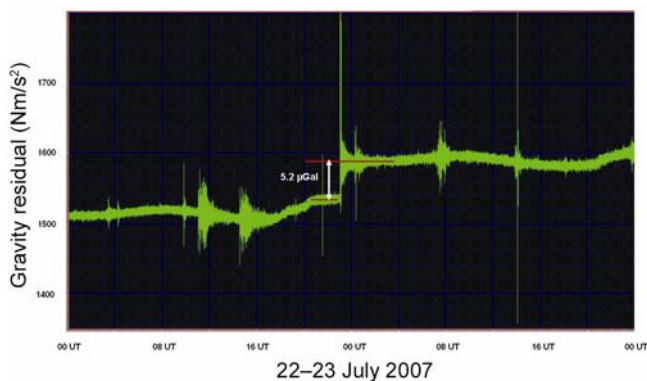


Figure 5. Co-seismic gravity step jump of 5.2 μGal recorded at Ghuttu in association with M 4.9 Kharsali earthquake.

response to the stress-induced deformation or due to the opening of micro-cracks has been invoked to explain anomalous radon concentrations associated with seismic activity^{46–48}. The changes in underground fluid flow may account for anomalous changes in radon concentrations⁴⁹. It is well documented that emanation and transport of radon in the rock matrix are affected by meteorological parameters like rainfall, soil moisture, pressure, temperature, etc. Several numerical methods are being used to characterize, often the site specific, background variability and isolate earthquake-related changes with varying success^{50–52}.

Given the above rationale and background knowledge, monitoring of ²²²radon at Ghuttu^{53,54} was carried out using

a gamma-ray radon monitoring probe based on $1.5'' \times 1.5''$ NaI scintillation. Measurements of radon concentration were carried out at two positions in a borehole dug to a depth of 68 m. In the operational system, the first radon-sensing probe was positioned at a depth of 10 m recording radon from the air column above the seasonally varying water level. The second probe was always submerged in water at a depth of 50 m probing radon concentration in water. In addition, simultaneous recordings of environmental variables such as atmospheric pressure, temperature, rainfall and groundwater level were made at the sampling interval of 15 min. The early examination of radon variations in closed air column showed a number of sporadic fluctuations (Figure 6), but two sharp bell changes marked by well-developed negative and positive excursions were distinct features around the Kharsali earthquake⁵³. The magnitudes of both positive and negative excursions in anomalous pattern were statistically significant as extreme values deviated by more than two standard deviations from the seasonal mean. The first of these anomalous patterns was observed on 26 June 2009, approximately 23 days before the occurrence of the Kharsali earthquake, whereas the second anomalous pattern was recorded a few hours before the event. In comparison, the radon concentration in water began to rise rapidly around 26 June 2009 and after attaining a peak around 30 June 2009 dropped exponentially to its normal value by 3 July 2009. Considering these to be characteristic of the precursory signal to an earthquake, an empirical relation incorporating the observed amplitude of the radon peak,

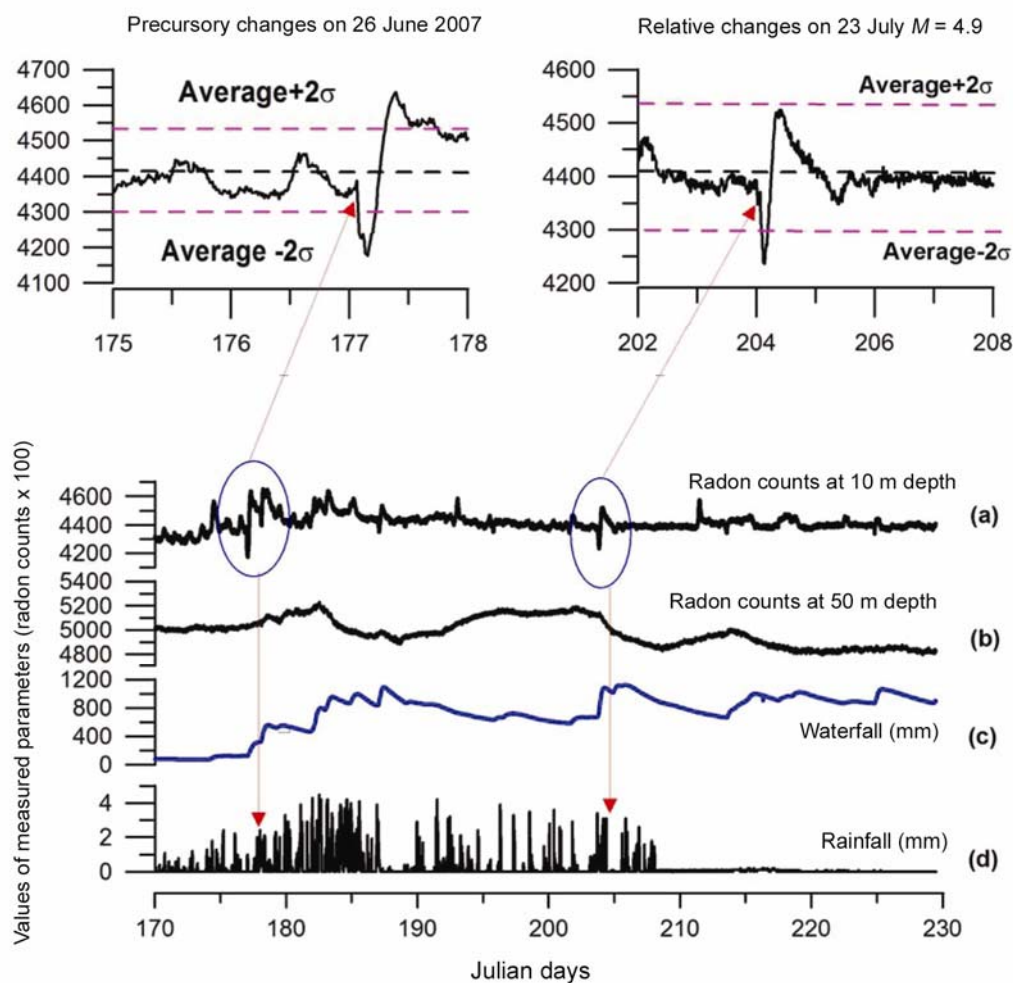


Figure 6. Radon concentration measured in (a) air column and (b) water column together with (c) water level in a deep bore hole and (d) rainfall recorded at MPGO, Ghuttu during 60 days (170–230 day numbers) interval of 2007. Bell-shaped anomaly in radon with sharp negative–positive impulse registered 22 days before and on the day of the Kharsali earthquake on 22 July 2007 (modified from Choubey *et al.*⁵³).

decay rate and average prevailing values of radon concentration estimated the magnitude of the impending earthquake close to M 4.6–4.7, in fair agreement with the observed magnitude of the Kharsali earthquake on 22 July 2007. While this example reinforced the physical rationale that there exists an association between stress build-up during an earthquake cycle and radon flux, further validation was emphasized in view of the fact that some of the recorded sharp changes in radon intensity coincided with intense rainfall, groundwater fluctuation as well as fluctuation in pressure and temperature. It has been demonstrated that the environmental factors by influencing the diffusion/advection/convection processes determine the escape and transport of radon⁵¹.

In the study by Choubey *et al.*⁵³ following the formulation described by Finkelstein *et al.*⁵¹, the influence of environmental/meteorological parameters on radon concentration was reduced by a single parameter defined by the sum of the correlation coefficients of radon with vari-

ous influencing metrological parameters. However, accumulating radon and meteorological and hydrological data at Ghuttu show complex variability, which introduces complexity in temporal behaviour of radon intensity. It was, therefore, considered crucial to quantify the radon variability in the geological setting of the study region so as to have a clear picture of background variability against which to compare potential radon anomalies as possible earthquake precursors. The time series of daily mean radon concentrations monitored at the MPGO during 2007–2009 is shown in Figure 7 whereas the nature of diurnal variation in radon recorded during different months is shown in Figure 8 (ref. 54). The strong seasonal variations with high values in the summer months (July–September) and low values in the winter months (December–February) closely followed the similar variations in atmospheric temperature and groundwater level fluctuations with time lag of a few days. The control of temperature gradient in the borehole on the

emission of radon was evident in the form of different patterns of daily variations. Examination and correlation with environmental factors has revealed that when surface atmospheric temperature was well below the water

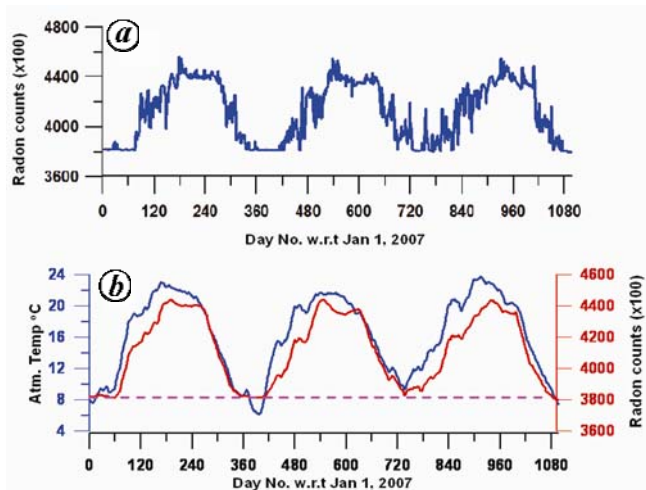


Figure 7. *a*, Plot of daily value of radon emission recorded at Ghuttu during 2007–2009. *b*, Plot of seasonal progression obtained from 31-day running mean of together with similarly derived atmospheric temperature.

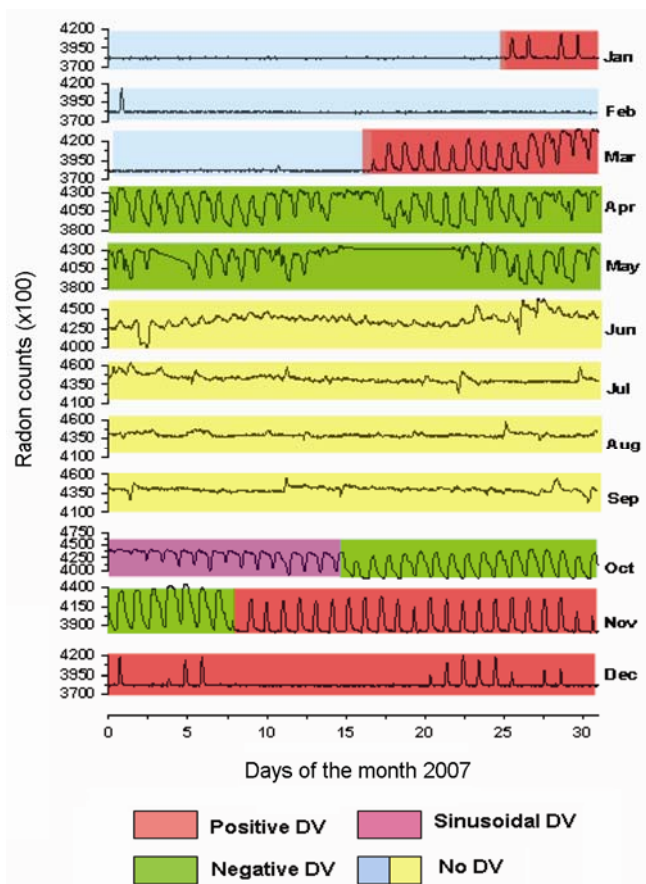


Figure 8. Monthly plots of diurnal variation in radon emission recorded in air column in a deep borehole at Ghuttu during 2007. Four distinct patterns of diurnal variations (DV) related to temperature and rainfall inequalities are seen.

temperature in the borehole, the latter showed a near constant value around 19°C throughout the year. Temperature gradients are not conducive to set up the convection currents for the emanation of radon to the surface (Figure 9). Thus explaining the absence of daily variation in radon concentration in winter⁵⁴. During the rainy season, following continuous rainfall, once the soil/rocks are saturated with water, the capping effect cuts-off the transfer of radon from the soil profile to the surface and vice versa and hence radon concentration shows fair stability at seasonal level and with no clear pattern of daily variation^{54,55}. During long pauses in rainfall, the soil begins to lose its saturation state due to evaporation and water flow is marked by jerky variability in radon concentration during the rainy season with no clear pattern of daily variation. During other periods of the year, the changing patterns in daily variation in radon counts can be reconciled by the form and amplitude of daily progression in atmospheric temperature in relation to groundwater temperature. This preliminary examination drives home the point that an accurate description of the effect of environmental variables is essential if we wish to decipher information related to stress/strain accumulation. Further quantification of meteorological and hydrological factors is in progress.

Anomalies in magnetic field

The localized changes in geomagnetic field intensity which in some manner appear to be associated with earthquake occurrence are named as seismomagnetic effect⁵⁶. Influence of stress build-up on the magnetization of rocks, piezomagnetic effect, is invoked as a possible physical mechanism. The stress-induced flow of fluids

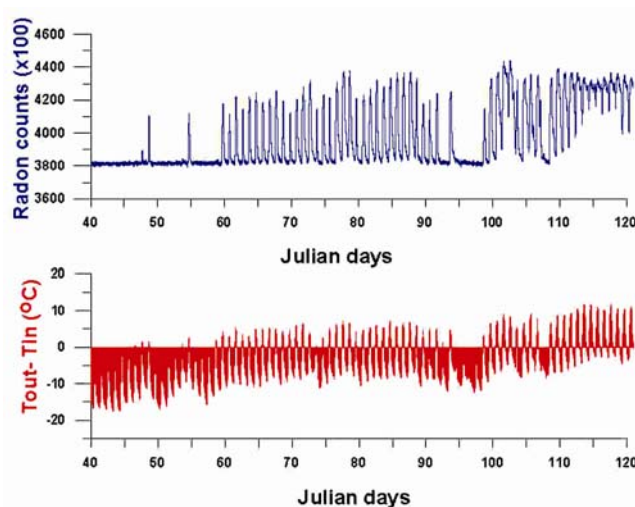


Figure 9. Temporal evolution of radon daily variation (top) in relation to temperature gradient defined by the difference in temperature within (T_{in}) and outside the bore hole (T_{out}) during the 100 days of the year 2008.

into dilatant zone of impending earthquake, produces relative charge separation, setting up streaming potential at the fluid–rock interface due to the difference in the mass of electron and ions. This electrokinetic phenomenon in turn induces electric current producing measurable changes both in electric and magnetic field at the earth's surface^{57,58}.

Total intensity of the geomagnetic field is measured by overhauser magnetometers of 0.01 nT sensitivity. Recorded geomagnetic fields are the vector sum of the internal main field and superposition of various transient fields originating from the magnetosphere, ionosphere, induction effects, crustal component and a small component of seismomagnetic origin. Since seismo-magnetic signal is weak, often the success of the experiment in documenting seismomagnetic anomalies relies on how precisely the magnetic variations of external origin can be estimated and eliminated. Taking advantage that external variations, primarily during the local night hours have their origin in magnetospheric processes, their behaviour at pairs of stations separated only by tens of kilometres would be identical and hence examination of data in differential mode permits residual field free from external variations. To achieve this, in addition to Ghuttu, overhauser magnetometers are being operated at two more sites, Bhatwari and Pipaldali (Figure 1b). Computation of differential variations, using an average of 181 1-min values, centred at local midnight, for pairs of stations shows residual fields with r.m.s. value of the order of only 0.4 nT. It is clear that seismomagnetic signals of magnitude 0.8 nT can be detected above 95% confidence by examining data in differential mode. As an example, Figure 10 shows the night-time differential plot of total magnetic field for three pairs of stations for the period 1 July–15 August 2007 encompassing the period of the Kharsali earthquake ($M_L = 4.9$) of 22 July 2007. It is seen that the differential plot for a pair of stations located on either of the epicentre across the MCT (Ghuttu–Bhatwari) shows a sudden fall of more than 1 nT in magnetic field intensity eight days before the earthquake, which recovered equally rapidly six days after the earthquake.

In an alternative approach, the method of principal component analysis was applied to each hour data at three stations to isolate prominent waveforms perhaps characterizing components of different source origins⁵⁹. Figure 9 shows the plot of square root of magnitude of the first three eigen values (λ). Since eigen values are a measure of the power of the measured signal, the square root plot depicts temporal variability of the amplitude of the principal wave form. As expected on physical considerations the time variation of the first eigen value (λ_1) follows quite closely the global geomagnetic index, K_p , indicating the control of magnetospheric processes. The variability of the second and third eigen values is invariably independent of global geomagnetic activity. It is noted that plots of λ_2 and λ_3 depict strong variability during the time

interval when the differential plot for Bhatwari–Ghuttu showed anomalous fall in total field intensity. As noted in Figure 10, the anomalous drop in total geomagnetic field is best developed in the differential plot of fields between Ghuttu and Bhatwari, and tends to be conspicuously absent in the differential plots of Bhatwari–Pipaldali; the source region of this anomalous change should be localized between Bhatwari and Ghuttu. Amongst the varied geology/tectonic setting, a common feature is that both sectors exhibit tectonic history of granitoid intrusion associated with Tertiary magmatism⁶⁰. On the basis of the mineral composition and petrophysical properties, both granitoid bodies at Bhatwari and Ghuttu are classified as S-type resulting from the melting of the middle crust⁶⁰. The petrologic and magnetic measurements revealed that paramagnetic minerals biotite and muscovite determine the bulk magnetic properties of granitoids, where single domain titanomagnetite mineral is the primary carrier of magnetization⁶¹. In the hypocentral depth of the Kharsali earthquake (~15 km), it is possible that in the thrust domain shear heating resulting in response to the accumulating stresses may locally bring the temperature close to the Curie temperature of titanomagnetite, i.e. in the range of 200–400°C (ref. 62). It is known that thermal agitation of magnetic minerals in rocks, close to the Curie temperature, can destroy the alignment of magnetic grains⁶³, which may be reflected in the form of perturbation of magnetic field intensity seen in the differential plot of the static total intensity (Figure 10) and dynamic waveform of the short-period fluctuations (Figure 11). Both static and dynamic fields resume their normal pattern once the thermally excited rocks return to normal conditions after the release of strains following the earthquake.

Anomalous electromagnetic emission

Anomalous electromagnetic (EM) emission in the ULF band (0.001–10 Hz) believed to be emanating from the elastic straining and/or micro-fracturing of crustal material during earthquake cycles has been widely documented from field data^{64,65}. Recent reviews^{14,17,66,67} trace the growth in field documentation, numerical approaches to isolate precursory signals, physical mechanisms, etc. A range of physical effects, e.g. electrokinetic effect, piezoelectric, microfracture electrification and displacement of crustal blocks of contrasting electrical conductivity are advanced to explain the observations (see Dudkin *et al.*⁶⁸ for review and references). Despite important leads and well-documented examples, seismo-EM precursors are not used in practical forecasting of earthquakes. Uyeda *et al.*¹⁷ have traced factors that deter applications of seismo-EM precursors in short-term prediction of earthquakes. The major impediments are: (i) chance detection of precursors as anomalous signals are confined to a small area around the epicentre and monitoring networks are not

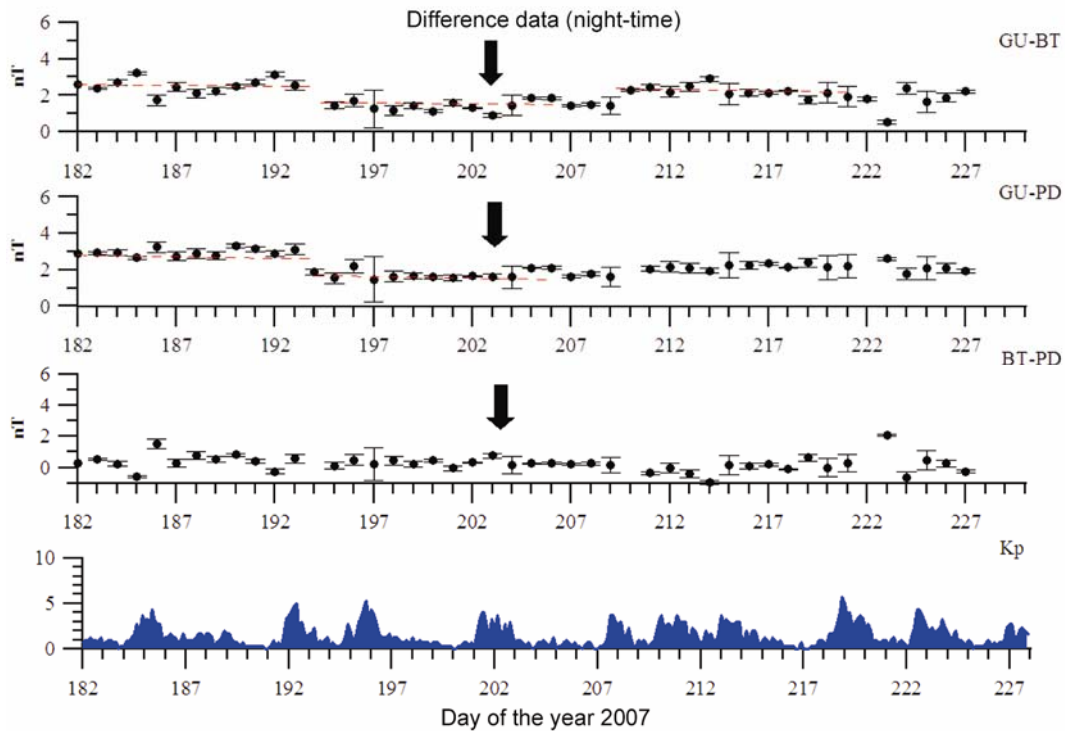


Figure 10. Difference plots of total geomagnetic field between three pairs of stations together with global geomagnetic index K_p . Difference plot for stations (Bhatwari–Ghuttu), located north and south of the epicentre of M_L 4.9 Kharsali earthquake, indicates reduction of geomagnetic field scanning 7 days before to 6 days after the earthquake on 22 July 2007.

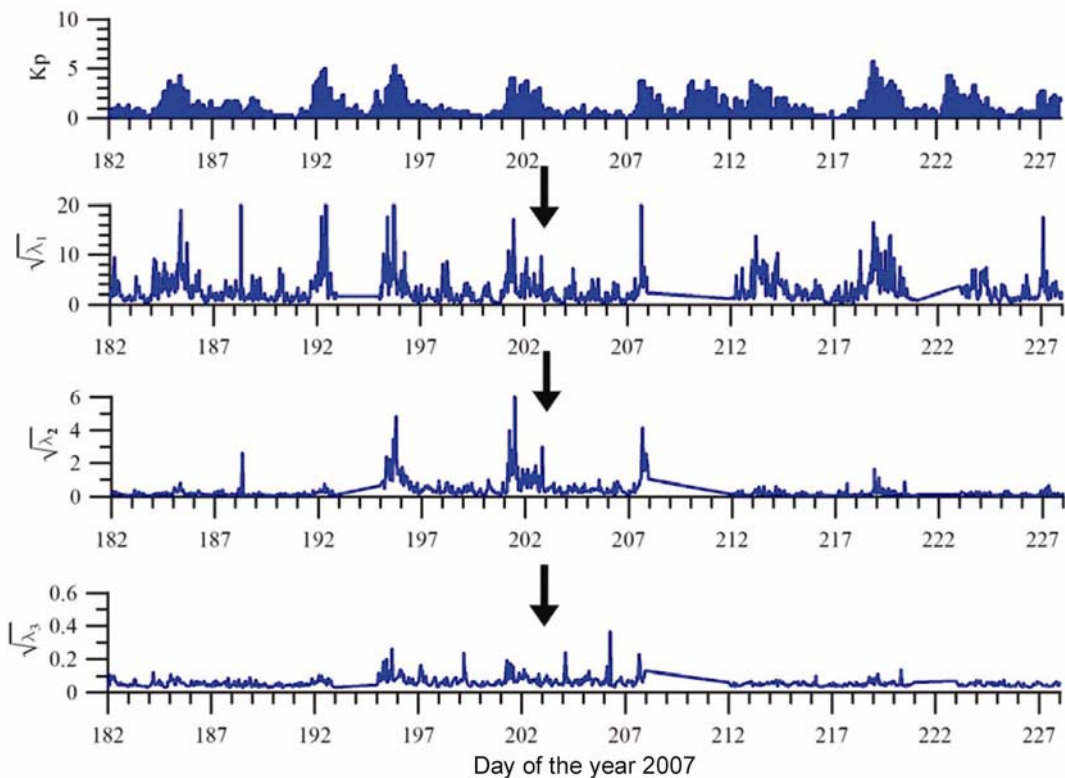


Figure 11. Time variation of three principal components (λ_1 , λ_2 , λ_3) of the geomagnetic field and related variations in association with the global geomagnetic activity index (K_p).

adequate to cover active zones; (ii) lack of robustness in isolating weak seismo-EM signals from strong background variations resulting from solar-wind–magnetosphere–ionosphere interactions; (iii) validation of the specific mechanism to explain particular features of field observations in varied tectonic settings and (iv) methodologies to locate source region of the seismo-EM emission from observations are still at infancy level.

Recognizing these deterrents, the plan and design of the EM experiment to collect data from the Garhwal Himalaya was guided by a pilot study carried out in the seismically active Koyna–Warna region, western India, that is a classical example of reservoir-triggered seismicity (for review, see Gupta⁶⁹). Following the *M* 6.3 earthquake on 10 December 1967, the area has remained seismoactive over the past four and half decades and source region of the seismicity is confined to a well defined belt of roughly 20 × 30 sq. km (ref. 25). This setting is unique for studying the peculiarities of the ULF magnetic field during the earthquake preparation process. The pilot study was aimed at testing a methodology⁶⁸ to locate the source region of seismo-EM signals. The fundamental of the proposed method is that geomagnetic field variations in the ULF band can be considered as a harmonic (periodic) function and as a consequence the locus of time-varying magnetic fields in three-orthogonal components traces out the polarization ellipse (PE) in space. The PE plane at any time contains the source of the magnetic field. If synchronous observations at two or multiple recording sites are available, the intersection line of PE planes from distant stations, should locate the source region of magnetic fields. In the test application of this principle in the Koyna–Warna sector, a pair of stations, one at Koyna within the limits of focused seismic zone and another station ~ 100 km away was operated at the Shivaji University, Kolhapur during April–May 2006. Extremely low-noise LEMI-30 magnetometers procured for installation at MPMGO, Ghattu were deployed at both stations. The magnetometers measure three-orthogonal components in the frequency range 0.001–32 Hz at selectable sampling interval. The amplitude and phase in X, Y and Z for a pre-defined frequency band (0.001–0.5 Hz) were used to calculate the parameters of PE for both measuring sites. For such a pair of stations, separated only by about 100 km, the distant source current system would produce near-identical variations and hence the ratio of major axes of PE dominated by magnetospheric and ionospheric fields will be close to unity, whereas magnetic fields with PE major axes ratio exceeding the critical threshold, say a value 2, can be ascribed to the possible seismo-EM precursory signals. The success of this criterion in discriminating the ULF signals of seismo-EM origin from the highly variable natural EM fields of solar–terrestrial sources was evident as PE for a number of ULF signals qualifying this criterion preceding two moderate earthquakes that occurred during the obser-

vation interval cluttered in the source region of the Koyna seismic activity. Approximating the plane of intersection as elementary magnetic dipole, the magnetic moment and orientation of magnetic dipole were determined by inversion of observed magnetic field. The computed azimuth of the seismo-EM fields invariably aligned in the NNW–SSE direction. The alignment of this orientation with causative fault zone as well as fault plane solutions of the two earthquakes discussed here, reinforced that the dipole orientations defined by seismo-EM signals can be used to infer the source region related to the earthquakes. It has been also demonstrated⁷⁰ that the ratio of the major axis of PE at pairs of stations proves more effective in the determination of weak seismo-EM signals from natural EM fields compared to the more commonly adopted indices of the polarization ratio⁶⁴ and fractal dimension^{65,71}. Given these developments to overcome some major deterrent in characterizing the true nature of the seismo-EM signals, monitoring of EM emission has commenced by establishing three stations in triangular configuration (Figure 1 *b*). The upcoming and functional hydroelectric dams are a major source of EM noise. Therefore, final selection of sites was achieved after complete testing for the background noise. The geometrical configuration is designed to target the Gaurikund–Tapovan area (Figure 2), which based on the clustering pattern in micro-earthquake activity is identified as the possible location for future large earthquakes²³. Given that on theoretical consideration seismo-EM can be detected only up to a distance of 100–150 km, in order to optimize the signals, no pair of stations is separated by 100 km. Concurrent recordings using the LEMI-30 magnetometer have commenced recently and data are being processed on the lines of the pilot experiment in Koyna.

Looking forward

The critical analysis of geophysical time series indicates that the time-variability of the gravity field is influenced by soil moisture and water-table fluctuations; flux of radon emission is strongly dependent on environmental factors like temperature and hydrology. These influences are the major deterrents in the isolation of weak precursory signals. However, data recorded since the inception of the observatory have proved critical in identifying the parameters determining the time variability of each time series. This quantification has been benefitted by the thoughtful selection and recording of meteorological and hydrological parameters that influence the various geophysical signals. Having recognized this, the next execution phase of the programme involves establishing physical and statistical models to estimate and eliminate effects of solar–terrestrial, hydrological/environmental factors on different geophysical time series. Some test applications in progress demonstrate that if effects of

environment and hydrology are not recognized and corrected for some perturbations, they will falsely be identified as earthquake precursors. On the other extreme, some precursory signals are masked by factors other than stress-induced changes.

Critical scrutiny of different time series has revealed certain precursory or co-seismic changes in association with the M 4.9 Kharsali earthquake. However, the physical factors/mechanisms producing changes in different parameters require validation. For example, the extent to which observed co-seismic changes in gravity fields are caused by the fault dislocation or by co-seismic volumetric strain changes needs to be established. Similarly, whether observed radon anomalies are related to earthquake occurrence or are an interplay of environmental parameters needs to be proved by more rigorous modelling. Clearly, this is an area requiring future focus. The most promising part is that certain emerging trends can be confirmed by cross-validation. For example, it would be interesting to check whether the step-like changes noted in the geomagnetic field could be linked with the thermal anomalies deciphered from satellite data^{72–75}. There are a number of convincing examples that thermal anomalies in the form of abrupt changes in surface temperature of the order of 3–7°C occur around 1–13 days prior to an earthquake and disappear a few days after the event⁷⁶. Close correspondence between thermal and geomagnetic field changes may strengthen the physical hypothesis that geomagnetic anomalies recorded in association with the Kharsali earthquake may be manifestations of thermal agitation in the alignment of magnetic grains due to increased temperature at seismogenic depths. Similarly, whether the long-term trend seen in the gravity field recorded during 2007–10 is simply an artefact of the drift behaviour of the gravity measuring system or is a manifestation of the mass distribution in rocks due to the stress built up, can be checked by the continuous GPS data collected at MPGO. Such cross-validation of multi-parameteric observations may well define the future path of precursory research^{13,77}. Further, as the largest earthquake recorded so far around MPGO was of magnitude close to 5, experience from other regions has shown that earthquake precursors with amplitude well above the equipment sensitivity and background noise are expected to be seen for earthquakes with $M \geq 6$. The major advantages of the multi-parameter approach crafted in the National Programme on Earthquake Precursors would be realized if recordings are continued for a long time, as envisaged originally in the project mission document.

1. Khattri, K. N. and Tyagi, A. K., Seismicity patterns in the Himalayan plate boundary and identification of the areas of high seismic potential. *Tectonophysics*, 1983, **96**, 281–297.
2. Rikitake, T., Probability of a great earthquake to recur in the Tokai district, Japan: reevaluation based on newly-developed paleoseismology, plate tectonics, tsunami study, micro-seismicity

- and geodetic measurements. *Earth Planets Space*, 1999, **51**, 147–157.
3. Stein, R. S., Barka, A. A. and Dieterich, J. H., Progressive failure on the North Anatolian fault since 1939 by earthquake stress triggering. *Geophys. J. Int.*, 1997, **128**, 594–604.
 4. Kossobokov, V. G., Romashkova, L. L., Keilis-Borok, V. I. and Healy, J. H., Testing earthquake prediction algorithms: statistically significant real-time prediction of the largest earthquakes in the Circum-Pacific, 1992–1997. *Phys. Earth Planet. Inter.*, 1999, **111**, 187–196.
 5. Keilis-Borok, V. I. and Soloviev, A. A. (eds), *Nonlinear Dynamics of the Lithosphere and Earthquake Prediction*, Springer-Verlag, Heidelberg, 2003, p. 335.
 6. Kagan, Y. Y. and Jackson, D. D., Global earthquake forecasts. *Geophys. J. Int.*, 2011, **184**, 759–776; doi: 10.1111/j.1365-246X.2010.04857.x
 7. Bilham, R., Gaur, V. K. and Molnar, P., Himalayan seismic hazard. *Science*, 2001, **293**, 1442–1444.
 8. Manaker, D. M. *et al.*, Interseismic plate coupling and strain partitioning in the northeastern Caribbean. *Geophys. J. Int.*, 2008, **174**, 889–903; doi: 10.1111/j.1365-246X.2008.03819.x
 9. Lomnitz, C., *Fundamentals of Earthquake Prediction*, John Wiley, New York, 1994, p. 326.
 10. Andrews, R. A., The Parkfield earthquake prediction of October 1992: the emergency services response. *Earthq. Volcanoes*, 1992, **23**, 170–174.
 11. Bakun, W. H. and Lindh, A. G., The Parkfield, CA earthquake prediction experiment. *Science*, 1985, **229**, 619–624.
 12. Langbein, J. *et al.*, Preliminary report on the 28 September 2004 M 6.0 Parkfield, California earthquake. *Seismol. Res. Lett.*, 2005, **76**, 10–26.
 13. Varotsos, P. A., *The Physics of Seismic Electric Signals*, Terra Publ, Tokyo, Japan, 2005, p. 338.
 14. Uyeda, S. and Park, S., Recent investigations of electromagnetic variations related to earthquakes. *J. Geodyn.*, 2002, **33**, 377–570.
 15. Geller, R., Debate on ‘VAN’. *Geophys. Res. Lett.*, 1996, **23**, 1291–1452.
 16. Cicerone, R. D., Ebel, J. E. and Britton, J., A systematic compilation of earthquake precursors. *Tectonophysics*, 2009, **476**, 371–396; doi: 10.1016/j.tecto.2009.06.008.
 17. Uyeda, S., Nagao, T. and Kamogawa, M., Short-term earthquake prediction: current status of seismo-electromagnetics. *Tectonophysics*, 2009, **470**, 205–213.
 18. Scholz, C. H., Sykes, L. R. and Agarwal, Y. P., Earthquake prediction: a physical basis. *Science*, 1973, **181**, 803–810.
 19. Banerjee, P. and Burgmann, R., Convergence across the northwest Himalaya from GPS measurement. *Geophys. Res. Lett.*, 2002, **29**, 1652–1655; doi: 10.1029/2002GL015184
 20. Pandey, M. R., Tandukar, R. P., Avouac, J. P., Lave, L. and Massot, J. P., Interseismic strain accumulation in the Himalayan crustal ramp in Nepal. *Geophys. Res. Lett.*, 1995, **22**, 741–754.
 21. Lyubushin, A. A., Arora, B. R. and Kumar, N., Investigation of seismicity in western Himalaya. *Russ. J. Geophys. Res.*, 2010, **11**, 27–34.
 22. Arora, B. R., Naresh Kumar, Sobolev, G. A., Lyubushin, A. A., Smirnov, V. B., Ponomarev, A. V. and Zavyalov, A. D., Precursory seismic markers to the 1999 – Chamoli Earthquake, Garhwal Himalaya. *J. Asian Earth Sci.*, 2011 (communicated).
 23. Paul, A. and Sharma, M. L., Recent earthquake swarms in Garhwal Himalaya: a precursor to moderate to great earthquakes in the region. *J. Asian Earth Sci.*, 2011, **42**, 1179–1186.
 24. Huang, Q., Search for reliable precursors: a case study of the seismic quiescence of 2000 western Tottori prefecture earthquake. *J. Geophys. Res.*, 2006, **111**, B04301, doi:10.1029/2005JB003982.
 25. Gupta, H. K. *et al.*, Earthquake forecast appears feasible at Koyna, India. *Curr. Sci.*, 2007, **93**, 843–848.

26. Papadimitriou, P., Identification of seismic precursors before large earthquakes: Decelerating and accelerating seismic patterns. *J. Geophys. Res.*, 2008, **113**, B04306; doi: 10.1029/2007JB005112.
27. Murru, M., Console, R. and Falcone, G., Real time earthquake forecasting in Italy. *Tectonophysics*, 2009, **470**, 214–223.
28. Kumar, N., Paul, A., Mahajan, A. K., Yadav, D. K. and Bora, C., 5.0 Mw Kharsali, Garhwal Himalaya earthquake of 23 July 2007: source characterisation and tectonic implications. *Curr. Sci.*, 2012, **102**(12), 1674–1682.
29. Arora, B. R., Kamal, Kumar, A., Rawat, G., Kumar, N. and Choubey, V. M., First observations of free oscillations of the earth (FOE) from Indian Superconducting gravimeter in Himalaya. *Curr. Sci.*, 2008, **95**, 1611–1617.
30. Tsoft, 2002; <http://www.astro.oma.be/SEISMO/TSOFT/tsoft.html>
31. Wenzel, H.-G., The nanogal software: earthtide data processing package ETERNA 3.3. *Marees Terr. Bull. Inf. Bruxelles*, 1996, **124**, 9425–9439.
32. Crossley, D. J., Jensen, O. G. and Hinderer, J., Effective barometric admittance and gravity residuals. *Phys. Earth Planet. Inter.*, 1995, **90**, 221–241.
33. Kroner, C. and Jahr, T., Hydrological experiments around the superconducting gravimeter at Moxa observatory. *J. Geodynamics*, 2006, **41**, 268–275.
34. Hasan, S., Troch, P. A., Boll, J. and Kroner, C., Modeling of hydrological effect on local gravity at Moxa, Germany. *J. Hydro-meteorol.*, 2006, **7**, 346–354; doi:10.1175/JHM488.1.
35. Kazama, T. and Okubo, S., Hydrological modeling of groundwater disturbances to observed gravity: theory and application to Asama Volcano, Central Japan. *J. Geophys. Res.*, 2009, **114**, B08402; doi: 10.1029/2009JB006391.
36. Nawa, K., Suda, N., Yamada, I., Miyajima, R. and Okubo, S., Co-seismic change and precipitation effect in temporal gravity variation at Inuyama, Japan: a case of the 2004 off the Kii peninsula earthquakes observed with a superconducting gravimeter. *J. Geodyn.*, 2009, **48**, 1–5.
37. Chia, Y., Chiu, J. J., Chiang, Y. H., Lee, T. P., Wu, Y. M. and Hrong, M. J., Implications of co-seismic groundwater level changes observed at multiple-well monitoring stations. *Geophys. J. Int.*, 2008, **172**, 293–301; doi: 10.1111/j.1365-246X.2007.03628.x.
38. Imanishi, Y., Sato, T., Higashi, T., Sun, W. and Okubo, S., A network of superconducting gravimeters detects sub-microgal co-seismic gravity changes. *Science*, 2004, **306**, 476–478.
39. Kim, J. W., Neumeier, J., Kim, T. H., Woo, I., Park, H. J., Jeong-Soo Jeon, J. S. and Kim, K. D., Analysis of Superconducting Gravimeter measurements at Mun Gyung station, Korea. *J. Geodyn.*, 2009, **47**, 180–190.
40. Hwang, C., Kao, R., Cheng, C. C., Huang, J. F., Lee, C. W. and Sato, T., Results from parallel observations of superconducting and absolute gravimeters and GPS at the Hsinchu station of Global Geodynamics Project, Taiwan. *J. Geophys. Res.*, 2009, **114** (B07406); doi: 10.1029/2008JB006195.
41. Gahalaut, K., Gahalaut, V. K. and Chadha, R. K., Analysis of co-seismic water-level changes in the wells in the Koyna–Warna region, Western India. *Bull. Seismol. Soc. Am.*, 2010, **100**, 1389–1394; doi: 10.1785/0120090165.
42. Sadovsky, M. A. *et al.*, The processes preceding strong earthquakes in some regions of Middle Asia. *Tectonophysics*, 1972, **14**, 195–307.
43. Igarashi, G. *et al.*, Groundwater radon anomaly before the Kobe earthquake in Japan. *Science*, 1995, **269**, 60–61; doi: 10.1126/science.269.5220.60.
44. Virk, H. S., Walia, V. and Kumar, N., Helium/radon precursory anomalies of Chamoli earthquake, Garhwal Himalaya, India. *J. Geodyn.*, 2001, **31**, 201–210.
45. Walia, V., Virk, H. S., Yang, T. F., Mahajan, S., Walia, M. and Bajwa, B. S., Earthquake prediction studies using radon as a precursor in N-W Himalayas, India: a case study. *Terr. Atmos. Ocean. Sci.*, 2005, **16**, 775–804.
46. Ghosh, D., Deb, A. and Sengupta, R., Anomalous radon emission as precursor of earthquake. *J. Appl. Geophys.*, 2009, **69**, 67–81.
47. Thomas, D. M., Geochemical precursors to earthquake. *Pure Appl. Geophys.*, 1988, **126**, 241–265.
48. Chyi, L. L., Quick, T. J., Yang, T. F. and Chen, C.-H., The experimental investigation of oil gas radon migration mechanisms and its implication in earthquake forecast. *Geofluids*, 2010, **10**, 556–563.
49. Steinitz, G., Begin, Z. B. and Gazit-Yaari, N., A statistically significant relation between Rn flux and weak earthquakes in the Dead Sea rift valley. *Geology*, 2003, **31**, 505–508.
50. Zmazek, B., Zivcic, M., Todorovski, L., Dzeroski, S., Vaupotic, J. and Kobal, I., Radon in soil gas: how to identify anomalies caused by earthquakes. *Appl. Geochem.*, 2005, **20**, 1106–1119.
51. Finkelstein, M., Eppelbaum, L. V. and Price, C., Analysis of temperature influences on the amplitude-frequency characteristics of Rn gas concentration. *J. Environ. Radioactivity*, 2006, **86**, 251–270.
52. Francesco, S. De, Tommasone, F. P., Cuoco, E., Verrengia, G. and Tedesco, D., Radon hazard in shallow groundwater: amplification and long term variability induced by rainfall. *Sci. Total Environ.*, 2010, **208**, 779–789; doi: 10.1016/j.scitotenv.2009.11.024.
53. Choubey, V. M., Kumar, N. and Arora, B. R., Precursory signatures in the radon and geo-hydrological borehole data for M 4.9 Kharsali earthquake of Garhwal Himalaya. *Sci. Total Environ.*, 2009, **407**, 5877–5883.
54. Choubey, V. M., Arora, B. R., Barbosa, S. M., Kumar, N. and Kamra, L., Seasonal and daily variation of radon at 10 m depth in borehole, Lesser Garhwal Himalaya, India. *J. Appl. Radiat. Isot.*, 2011, **69**, 1070–1078; doi: 10.1016/j.2011.03.027.
55. Neilson, K. K., Rogers, V. C. and Gee, G. W., Diffusion of radon through soils: a pore distribution model. *Soil Sci. Soc. Am. J.*, 1984, **48**, 482–487.
56. Johnston, M. J. S., Review of electric and magnetic fields accompanying seismic and volcanic activity. *Surv. Geophys.*, 1997, **18**, 441–475.
57. Fitterman, D. V., Electrokinetic and magnetic anomalies associated with dilatants regions in a layered earth. *J. Geophys. Res.*, 1978, **83**, 5923–5928.
58. Dobrovolsky, I. P., Gershenzon, N. I. and Gokhberg, M. B., Theory of electrokinetic effects occurring at the final stage in the preparation of a tectonic earthquake. *Phys. Earth Planet. Inter.*, 1989, **57**, 144–156.
59. Hattori, K., Serita, A., Yoshino, C. and Hayakawa, M., Singular spectral analysis and principal component analysis for signal discrimination of ULF geomagnetic data associated with 2000 Izu Island earthquake swarm. *Phys. Chem. Earth*, 2000, **31**, 281–291.
60. Islam, R., Ahmed, T. T. and Khanna, P. P., An overview of the granitoids of the NW Himalaya. *Himalayan Geol.*, 2005, **26**, 49–60.
61. Sharma, R., Gupta, V., Arora, B. R. and Sen, K., Petrophysical properties of the Himalayan granitoids: implication on composition and source. *Tectonophysics*, 2011, **497**, 23–33.
62. Butler, R. F., *Magnetic Domains to Geologic Terrenes*, Blackwell Scientific Publications, 1992, p. 319.
63. Dunlop, D. J. and Özdemir, Ö., *Rock Magnetism: Fundamentals and Frontiers*, Cambridge University Press, Cambridge, 1997, p. 573.
64. Hayakawa, M., Kawate, R., Molchanov, O. A. and Yumoto, K., Results of ultra-low-frequency magnetic field measurements during the Guam earthquake of 8 August 1993. *Geophys. Res. Lett.*, 1996, **23**, 241–244.
65. Hayakawa, M., Itoh, T. and Smirnova, N., Fractal analysis of ULF geomagnetic data associated with the Guam earthquake on 8 August 1993. *Geophys. Res. Lett.*, 1999, **26**, 2797–2800.

66. Molchanov, O. A. and Hayakawa, M., *Seismo-electromagnetics and Related Phenomena: History and Results*, TERRAPUB, Tokyo, 2008, p. 189.
67. Hayakawa, M. (ed.), *The Frontier of Earthquake Prediction Studies*, Nihon-senmontosho-Shuppan, Tokyo, 2112, p. 785.
68. Dudkin, F., Rawat, G., Arora, B. R., Korepanov, V., Leontyeva, O. and Sharma, A. K., Application of polarization ellipse technique for analysis of ULF magnetic fields from two distant stations in Koyna–Warna seismoactive region, West India. *Nat. Hazards Earth Syst. Sci.*, 2010, **10**, 1–10; doi:10.5194/nhess-10-1-2010.
69. Gupta, H. K., A review of recent studies of triggered earthquakes by artificial water reservoirs with special emphasis on earthquakes in Koyna, India. *Earth Sci. Rev.*, 2002, **58**, 279–310.
70. Arora, B. R., Rawat, G. and Mishra, S. S., Indexing of ULF electromagnetic emission to search earthquake precursors. In *The Frontier of Earthquake Prediction Studies* (ed. Hayakawa, M.), Nihon-senmontosho-Shuppan, Tokyo, 2012, pp. 346–362.
71. Ida, Y. and Hayakawa, M., Fractal analysis for the ULF data during the 1993 Guam earthquake to study prefracture criticality. *Nonlinear Process. Geophys.*, 2006, **13**, 409–412.
72. Tronin, A., Hayakawa, M. and Molchanov, O. A., Thermal IR satellite data application for earthquake research in Japan and China. *J. Geodyn.*, 2002, **33**, 519–534.
73. Dey, S. and Singh, R. P., Surface latent heat flux as an earthquake precursor. *Nat. Hazards Earth Syst. Sci.*, 2003, **3**, 749–755.
74. Saraf, A. K. and Choudhury, S., NOAA–AVHRR detects thermal anomaly associated with 26 January, 2001 Bhuj earthquake, Gujarat, India. *Int. J. Remote Sensing*, 2005, **26**, 1065–1073.
75. Genzano, N., Aliano, C., Filizzola, C., Pergola, N. and Tramutoli, V., A robust satellite technique for monitoring seismically active areas: the case of Bhuj–Gujarat earthquake. *Tectonophysics*, 2007, **431**, 221–230.
76. Saradjian, M. R. and Akhoondzadeh, M., Prediction of the date, magnitude and affected area of impending strong earthquakes using integration of multi precursors earthquake parameters. *Nat. Hazards Earth Syst. Sci.*, 2011, **11**, 1109–1119.
77. Ouzounov, D., Hattori, K. and Liu, J. Y., Validation of earthquake precursors–VESTO. *J. Asian Earth Sci.*, 2011, **41**, 369–370.

ACKNOWLEDGEMENTS. Setting up of the MPMGO was supported by the Ministry of Earth Sciences (MoES), Government of India. We thank Dr Shilesh Nayak, the Secretary to Govt of India, MoES for his support and motivation in achieving the challenging mission. The innumerable discussions with the Chairman and members of the Project Management Board in finalizing the design, selection of equipment and operational strategies are acknowledged. The Government of Uttarakhand facilitated the allocation of land. The Head, Geosciences and Coordinator at the MoES provided support and guidance. Continued support and encouragement provided by the host institutions is appreciated. B.R.A. thanks CSIR, New Delhi for award of the Emeritus Scientist Fellowship.

Received 23 April 2012; accepted 9 October 2012